

© Copyright 2022

Pedro Angulo-Umana

The Enhancement of Precipitation due to Mesoscale Convective Organization

Pedro Angulo-Umana

A thesis
submitted in partial fulfillment of the
requirements for the degree of

Master of Science

University of Washington

2022

Committee:

Daehyun Kim

Dale Durran

Dargan Frierson

Program Authorized to Offer Degree:

Atmospheric Sciences

University of Washington

Abstract

The Enhancement of Precipitation due to Mesoscale Convective Organization

Pedro Angulo-Umana

Chair of the Supervisory Committee:
Daehyun Kim
Department of Atmospheric Sciences

In the tropics, extreme precipitation events are often caused by mesoscale systems of organized, spatially clustered deep cumulonimbi, posing a substantial risk to life and property. While the clustering of convective clouds has been thought to strengthen precipitation intensity, no quantitative estimates of this hypothesized enhancement exist. In this study, we use observational data to demonstrate that this enhancement of precipitation intensity does indeed exist. After isolating the effects of mesoscale convective clustering on precipitation, we find that strongly clustered convection precipitates about 47% more intensely than weakly clustered convection. We further show that this enhancement is primarily attributable to an increase in convective precipitation intensity when the environment is less than 70% saturated, with increases in stratiform cloud cover being of equal or greater importance when the environment is closer to saturation. We show that this convective-stratiform transition is a consequence of the invariance of tropical convective and stratiform rain fractions to the degree of mesoscale convective clustering present. Our results are intended to serve as observational constraints for the representation of mesoscale organized convective systems in numerical models, aiding in making more accurate prediction of extreme precipitation events.

TABLE OF CONTENTS

List of Figures	2
List of Tables	3
Chapter 1. Introduction	6
Chapter 2. Data & Methods	9
2.1 Datasets	9
2.1.1 TRMM Satellite Observations	9
2.1.2 ERA5 Reanalysis	11
2.2 Methods.....	11
2.2.1 Quantifying Mesoscale Convective Organization	11
2.2.2 Isolating Mesoscale Convective Organization.....	15
Chapter 3. Results and Discussion.....	17
3.1 The Enhancement of Tropical Precipitation Intensity	17
3.2 Convective and Stratiform Components of Enhancement.....	21
Chapter 4. Conclusions	27
Chapter 5. References	29

LIST OF FIGURES

Figure 1.1: A top down view of a typical MCS. (a) An idealized sketch of radar reflectivity, with localized maxima representing deep convective cores and a large region of stratiform precipitation. (b) A sketch of the convective and stratiform regions of an MCS. From Houze (1997).....	7
Figure 2.1: Example of a scene as observed by TRMM. The $2^\circ \times 2^\circ$ scene shown is characterized by (left) 2A25 near-surface precipitation intensity and (right) 2A23 rain type classification.	9
Figure 3.1: Bin-mean precipitation intensity. SF bins are 1%, and CAF bins are 0.5%..	17
Figure 3.4: The enhancement of precipitation attributed to (top left) strengthened convective precipitation intensity, (top right) strengthened stratiform precipitation intensity, (bottom left) larger stratiform area fraction, and (bottom right) covariance between stratiform area fraction and stratiform precipitation intensity. Each component is computed using Eq. 3.3.	23
Figure 3.5: Average contribution of convective and stratiform components of PEMC. Also shown are mean convective and stratiform rain fractions. We observe that the convective and stratiform contributions to PEMC are strongly correlated with the convective and stratiform rain fractions, respectively.	24
Figure 3.6: Change in (top left) convective and (bottom left) stratiform rain fractions between strongly and weakly organized scenes. The average change over CAF bins is shown in the right panel (top convective, bottom stratiform)s. The difference between the CRF of strongly and weakly clustered is small, with a mean difference in CRF of 3.3%. The difference between the two is greatest in the range $60\% < SF < 80\%$	25

LIST OF TABLES

Table 2.3: List of proposed indices to quantify degree of convective organization 12

ACKNOWLEDGEMENTS

I would first like to acknowledge my advisor, Daehyun Kim, for his guidance in completing the work shown in this thesis. I would also like to thank my committee members, Dale Durran and Dargan Frierson, for their support and willingness to serve on my committee. I am also indebted to my groupmates for their help in refining the arguments made in this thesis.

I would finally like to acknowledge friends and family for providing a good reason to leave work every evening.

DEDICATION

For Mel

Chapter 1. INTRODUCTION

Mesoscale Convective Systems (MCSs; Houze, 2004) are tropical weather systems which comprise an ensemble of spatially clustered deep cumulonimbus clouds. MCSs are also characterized by their anvil cloud, which forms from the detrainment of water out of the cumuli into the high and mid troposphere. The rainy portion of an MCSs are composed of a *convective region*, where precipitation falls as a result of the deep convection, and a *stratiform region*, where detrained water and ice grow via vapor deposition before dropping (Rutledge and Houze, 1987; Houze, 1997). The precipitation over the convective region is typically much more intense than the stratiform precipitation that falls out of the rainy portion of the anvil cloud. Despite its lesser intensity relative to convective precipitation, the stratiform region is typically much larger than the convective region. As such, approximately 40% of tropical precipitation is stratiform in nature (Cheng and Houze, 1979; Leary, 1984; Schumacher and Houze, 2003). The total precipitation contribution of an MCS is the sum of the stratiform precipitation and the convective precipitation generated by the system.

MCSs have been shown to be of first order importance to the tropical hydrological cycle. MCSs have been shown to produce the majority of total precipitation that falls over the tropics (e.g., Nesbitt et al., 2006; Roca et al., 2014; Jaramillo et al., 2017). Changes in tropical rainfall climatology have been ascribed as the result of changes in MCS frequency (Tan et al., 2015). Larger-scale tropical convective systems, such as equatorial waves and the Madden-Julian Oscillation (MJO; Madden and Julian, 1972, 1971) are themselves made up of individual MCSs embedded within the synoptic scale envelope associated with the large-scale system (Nakazawa, 1988; Majda and Biello, 2004; Kiladis et al., 2009). Thus, MCSs can be conceptualized as a sort of “building block” of tropical convection. MCSs are the individual convective “atoms” that combine to form larger, more complex convective “molecules” like the MJO, Kelvin waves, and other tropical waves (Mapes et al., 2006). This leads to the MCS potentially serving as a bridge between short-term weather on the one hand and long-term climactic trends on the other. Understanding such *scale interactions*, as they are typically termed in the literature, remains an active area of research (e.g., Meehl et al., 2001).

Unfortunately, however, MCSs remain very poorly represented in numerical models for weather and climate prediction. Very few operational global circulation models (GCMs) represent

MCSs (Rio et al., 2019). A primary reason for this lack of representation is the fact that the spatial and temporal scales at which MCSs exist are much smaller than what can be reliably resolved by a typical GCM. The typical size the cloud shield of an MCS is on the order of 100 km in one direction; a typical GCM grid cell has side lengths on the order of 250km-600km. A typical lifetime of an MCS is on the order of a dozen hours; most GCMs that are used for climate projections are run with timesteps much longer than an hour. This difference in scale is not unique to MCSs; many processes, from convection itself to ice microphysics, occur at scales smaller than a GCM's spatiotemporal resolution, but are still represented via parameterizations. However, there remains a lack of consensus on how best to represent the effects of mesoscale (or, as it is sometimes called in the context of GCM studies, *subgrid*) convective organization. In other words, while the effects of convection are often represented in GCMs via convective parameterization schemes, the effects caused by the organization of convection at the mesoscale are typically not represented by a scheme (Moncrieff, 2019). While typically not utilized in operational forecasting, several parameterizations and approaches have been proposed to incorporate the effects of mesoscale convective organization into GCMs (e.g., Donner, 1993; Moncrieff, 2004; Mapes and Neale, 2011; Park, 2014; Khouider and Moncrieff, 2015; Moncrieff et al., 2017; Moncrieff, 2019). While different proposed parameterizations may differ in their formulations and representations of mesoscale convective organization and its effects on the atmosphere, most schemes are formulated in terms of parameters (e.g., cloud lifetime, cold pool size and velocity, etc.) that often require

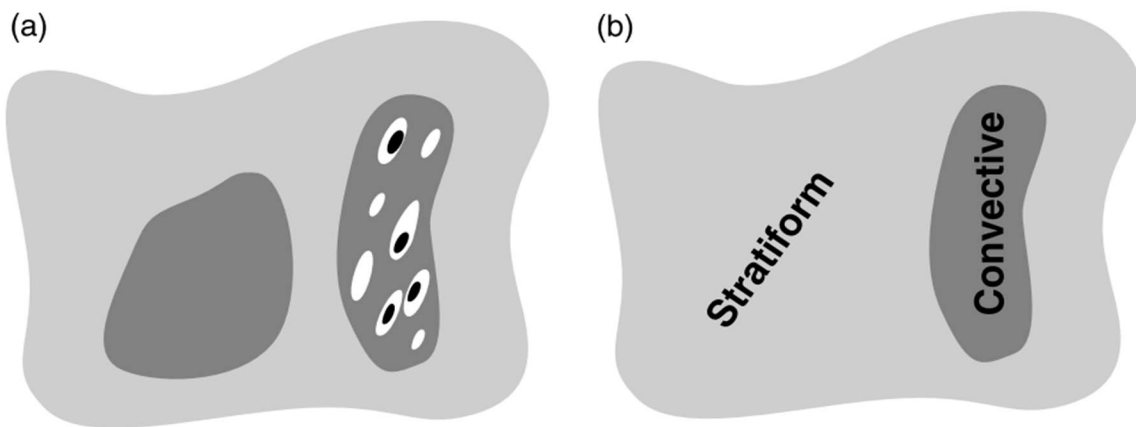


Figure 1.1: A top-down view of a typical MCS. (a) An idealized sketch of radar reflectivity, with localized maxima representing deep convective cores and a large region of stratiform precipitation. (b) A sketch of the convective and stratiform regions of an MCS. From Houze (1997)

hand-tuning. This tuning is often done without observationally based constraints to motivate or inform the adjustment of model parameters. Ideally, these parameterizations would be tuned and evaluated against observations beyond climatology, so as to ensure that the parameterization is faithfully capturing the multifaceted nature of convection and convective organization.

In this thesis we provide observationally based constraints on how mesoscale convective organization impacts tropical precipitation. We pose two questions that will be answered in this thesis:

1. Can we quantify the effects of mesoscale convective organization on tropical precipitation intensity?
2. How does mesoscale convective organization affect convective and stratiform processes?

The first question will provide a quantitative estimate of how much mesoscale convective organization can modulate precipitation intensity. Our aim in asking this question is to obtain an observationally based benchmark against which the performance of parameterizations of mesoscale convective organization may be evaluated. Furthermore, answering this question additionally help quantify the importance of mesoscale convective organization in determining tropical precipitation intensity.

The aim of the second question is to provide a process-level understanding of how the effects of mesoscale convective organization on precipitation intensity are mediated by convective and stratiform processes. This will provide some insight into what dynamical processes are important for understanding MCS dynamics. These findings can also serve as additional constraints for the development, tuning, and assessment of proposed subgrid organization schemes.

The following chapters are organized as follows: Chapter 2 details the data and methodology used to isolate and quantify the effects of mesoscale convective organization; Chapter 3 describes the enhancement of tropical precipitation intensity that can be associated with a greater degree of mesoscale convective organization, as well as how this enhancement differentially augments convective and stratiform precipitation; Chapter 4 states our conclusions, and provides ideas on future directions this work may take.

Chapter 2. DATA & METHODS

In this chapter, we detail the observational and reanalysis datasets utilized to answer the two questions posed in Chapter 1. We also describe how we objectively quantified the degree of convective organization present over tropical mesoscale domains, as well as how we isolated the effects of mesoscale convective organization from other confounding factors.

2.1 DATASETS

2.1.1 *TRMM Satellite Observations*

Observational data were derived from NASA Tropical Rainfall Measuring Mission (TRMM) Precipitation Radar (TRMM-PR) satellite observation datasets. The data are comprised of snapshots along the satellite's observational swath. Each snapshot has $0.05^\circ \times 0.05^\circ$ resolution on a regular Cartesian grid. The data are available from January 1, 1998 to December 31, 2013. Since we are interested in how convective organization augments convective organization over mesoscale domains, each TRMM snapshot is partitioned into disjoint $2^\circ \times 2^\circ$ cells, which we will call "scenes". Since each scene may not lie completely inside the observational swath, only scenes

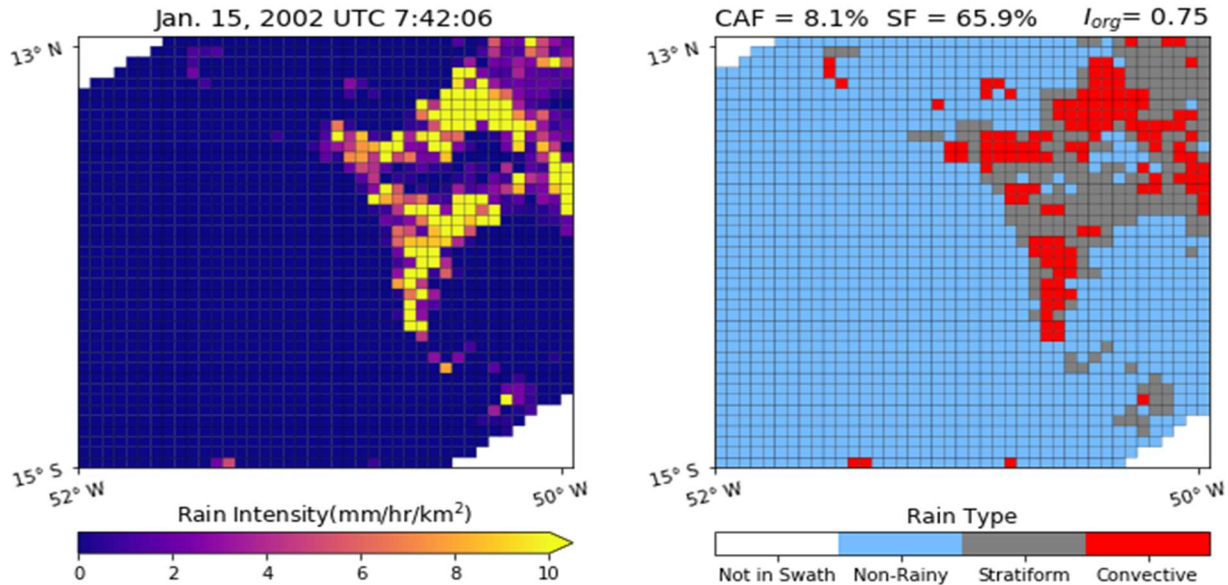


Figure 2.1: Example of a scene as observed by TRMM. The $2^\circ \times 2^\circ$ scene shown is characterized by (left) 2A25 near-surface precipitation intensity and (right) 2A23 rain type classification.

with more than 70% areal coverage are considered in our analysis. We further constrain our consideration to scenes that are over ocean. This allows us to neglect potential influences of orography or terrain on the organization and strength of convection. Scenes are selected from four regions selected from major tropical oceanic basins:

- The western Pacific Ocean, defined as the region bounded by 150° E to 190° E;
- The eastern Pacific Ocean, defined as the region bounded by 200° E to 240° E;
- The tropical Atlantic Ocean, defined as the region bounded by 319° E to 359° E;
- The central Indian Ocean, defined as the region bounded by 55° E to 95° E.

All regions are meridionally bounded between 15°N and 15°S. The total number of scenes considered in this study is 702,790.

To characterize the precipitation intensity and spatial distribution of convection over each scene, two TRMM products were utilized: surface rain rate estimates (2A25; Iguchi and Meneghini, 1994); and rain type classification (2A23; Awaka et al., 2009). Surface rain rate estimates are provided as estimates of the instantaneous intensity of precipitation near the surface. The rain type classification further classifies rainy pixels as either “convective”, “stratiform”, or “other”. The 2A23 algorithm by which this classification is performed is done by a vertical and horizontal profiling of the three-dimensional radar reflectivity as observed by TRMM-PR (V-method and H-method, respectively). The V-method is centered around the identification of bright band, a quasi-horizontal layer of strong reflectivity near the melting level (0° isotherm) that is characteristic of stratiform precipitation (e.g., Steiner et al., 1995; Houze, 1997). The H-method is similar to the method of Steiner et al. (1995), whereby convective pixels are identified as those with strong precipitation intensity (or equivalently, strong radar reflectivity) relative to their

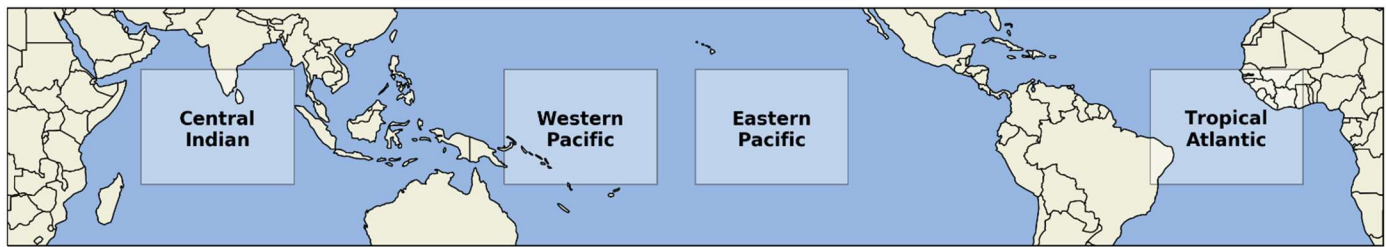


Figure 2.2: The four tropical oceanic regions from which TRMM scenes were selected. The boundaries of each of the above labelled regions are given in the text.

background. These two methods are performed in parallel and compared to generate a

classification of each rainy pixels as convective, stratiform, or “other”, with this last category serving as a catch-all classification for rainy pixels which cannot be confidently classified as either convective or stratiform via 2A23. As found in Schumacher and Houze (2003), “other” pixels are representative of noise, or precipitation aloft that does not reach the surface. The same study found that the precipitation associated with “other” pixels is a fraction of a percent of the total precipitation as measured by TRMM; as such, we can safely ignore this category of pixel, since our interest is in the augmentation of precipitation intensity associated with convective organization. Rainy pixels that are identified as undergoing convective precipitation by 2A23 will be called “convective pixels”; similarly, rainy pixels that are identified as undergoing stratiform precipitation by 2A23 will be called “stratiform pixels”.

2.1.2 *ERA5 Reanalysis*

Vertical profiles of temperature and specific humidity were obtained from fifth generation European Centre for Medium-Range Weather Forecasts (ECMWF) reanalyses (ERA5; Hersbach et al., 2020). The ERA5 data are provided at $0.25^\circ \times 0.25^\circ$ resolution at hourly timesteps. The vertical profiles used in this there are provided at pressure levels from 1000 hPa to 100 hPa with 100 hPa increments between levels. These profiles were used to compute the saturation fraction of the mesoscale domains under consideration (Section 2.2.2). Since the TRMM observations are not taken at regular time intervals, colocation of ERA5 data and TRMM data was performed by interpolating ERA5 data to the time of the corresponding TRMM observation. This was done for every TRMM observation considered in this study.

2.2 METHODS

2.2.1 *Quantifying Mesoscale Convective Organization*

There are several indices that have been proposed and used in the research literature for objectively quantifying the degree of convective organization present over a domain (Table 2.3). These indices generally consider organized convection to be convection which is tightly aggregated spatially. Several of the listed indices (for example, SCAI) have been shown to display undesired dependence on the number of convective elements present (Cheng et al., 2018; Xu et al., 2019). As such, for this study we used the “organization index”, or I_{org} , as defined in Tompkins

and Semie (2017). The organization index is computed by comparing the distribution of nearest-neighbor distances of N convective elements over a domain with area A to the distribution that would be expected from a random distribution of the same number of convective elements over the same area. For our study, the “convective elements” we consider are the rainy pixels identified as convective by the TRMM 2A23 dataset; other studies have used the geometric centroids of convective clusters (Stein et al., 2017; Tobin et al., 2012; Tompkins and Semie, 2017) or local minima of brightness temperature satellite data (Semie and Bony, 2020). We do not group adjacent convective pixels into single larger convective entities; given the large area encompassed by each TRMM pixel ($0.05^\circ \times 0.05^\circ \approx 25\text{km}^2$), doing so may artificially decrease the observed degree of convective organization by grouping distant convective systems together.

To formulate a quantitative definition of I_{org} , consider a scene with N convective pixels and an area A . Each convective element has a nearest-neighbor distance (NND) to another convective element. Let r_i be the NND of the i^{th} convective pixel. We thus have a list of N (potentially non-unique) NNDs, $\{r_1, \dots, r_N\}$. We can assume that this set is ordered so that $r_i \leq r_j$ when $i \leq j$. We define the nearest-neighbor cumulative density function (NNCDF) as the cumulative density function of the set of nearest-neighbor distances. That is, $NNCDF(r)$ is the fraction of convective elements with nearest-neighbor distance less than or equal to r . Let m_i be the number of convective elements with nearest-neighbors distance less than or equal to r_i . Thus, for $r \in [r_i, r_{i+1})$,

Table 2.3: List of proposed indices to quantify degree of convective organization

Short Name	Long Name	Reference
SCAI	Simple Convective Aggregation Index	Tobin et al., 2012
COP	Convective Organization Potential	White et al., 2005
I_{org}	Organization Index	Tompkins & Semie, 2017
MCAI	Modified SCAI	Xu et al. 2019

$$NNCDF(r) = \frac{m_i}{N}$$

From this definition, we can see that $NNCDF(r)$ is a piecewise constant function.

Consider now the cumulative distribution function of NNDs that would be expected if N convective pixels were randomly distributed about the scene. Suppose that each pixel has area δA . Thus there are $N_A = A/\delta A$ pixels, convective or otherwise, in the scene. The density of convective pixels, or equivalently the probability of each pixel to be convective, is

$$\lambda = \frac{N}{N_A} = \frac{N\delta A}{A}$$

Within distance r of each convective pixel, there are $\pi r^2/\delta A$ pixels. The expected fraction of convective pixels with a NND less than r (i.e., the cumulative distribution function of the randomly distributed convection) is equal to the probability that there is at least one convective pixel within distance r of any given convective pixel. This probability is complementary to the probability that there are *no* convective pixels within distance r of any given convective pixel. The probability that the NND of any given convective pixel is greater than r is thus

$$\mathcal{P}(NND > r) = (1 - \lambda)^{\frac{\pi r^2}{\delta A}} = \left(1 - \frac{N\delta A}{N_A}\right)^{\frac{\pi r^2}{\delta A}}$$

We can take the limit as $\delta A \rightarrow 0$, equivalent to assuming that the resolution of the scene is very fine, to simplify the above expression to

$$\mathcal{P}(NND > r) = e^{-\lambda\pi r^2}$$

Thus, the probability that there *is* a convective pixel within distance r , which is the cumulative distribution function of nearest-neighbor distances for random convection, is

$$NNCDF_{ran}(r; \lambda) = 1 - e^{-\lambda\pi r^2}, \quad (2.1)$$

equal to the expression given in Tompkins and Semie (2017).

As in Tompkins and Semie (2017), we can plot a parametric curve given by

$$\begin{aligned} x(r) &= NNCDF_{ran}(r; \lambda) \\ y(r) &= NNCDF(r) \end{aligned}$$

for $r \in [0, \infty)$, where $NNCDF(r)$ is the nearest neighbor cumulative density function for the scene under consideration, and $NNCDF_{rand}(r; \lambda)$ is the expected nearest neighbor cumulative

density function for a random distribution with density of convective pixels equal to the scene under consideration. The resultant curve is a piecewise constant function, with endpoints at (0,0) and (1,1). We define I_{org} as the area under this curve; I_{org} is thus bounded between 0 and 1. We note that if the scene's convective pixels were in fact randomly distributed, then this curve would lie along the diagonal $x = y$; thus we can ascribe meaning to the value of I_{org} by defining scenes with $I_{org} > 0.5$ as being "aggregated", or organized, and scenes with $I_{org} < 0.5$ as being "disaggregated", or disorganized. The larger I_{org} is, the stronger the degree of convective organization present over a given scene.

We can use the fact that the parametric curve used to define I_{org} is piecewise constant to express I_{org} exactly. The piecewise constant nature of this curve is due to the fact that $NNCDF(r)$ is piecewise constant as well. The area under this curve can thus be partitioned into several rectangles, the number of which corresponds to the number of unique NNDs in the scene. We can thus state that the area under the parametric curve is given by

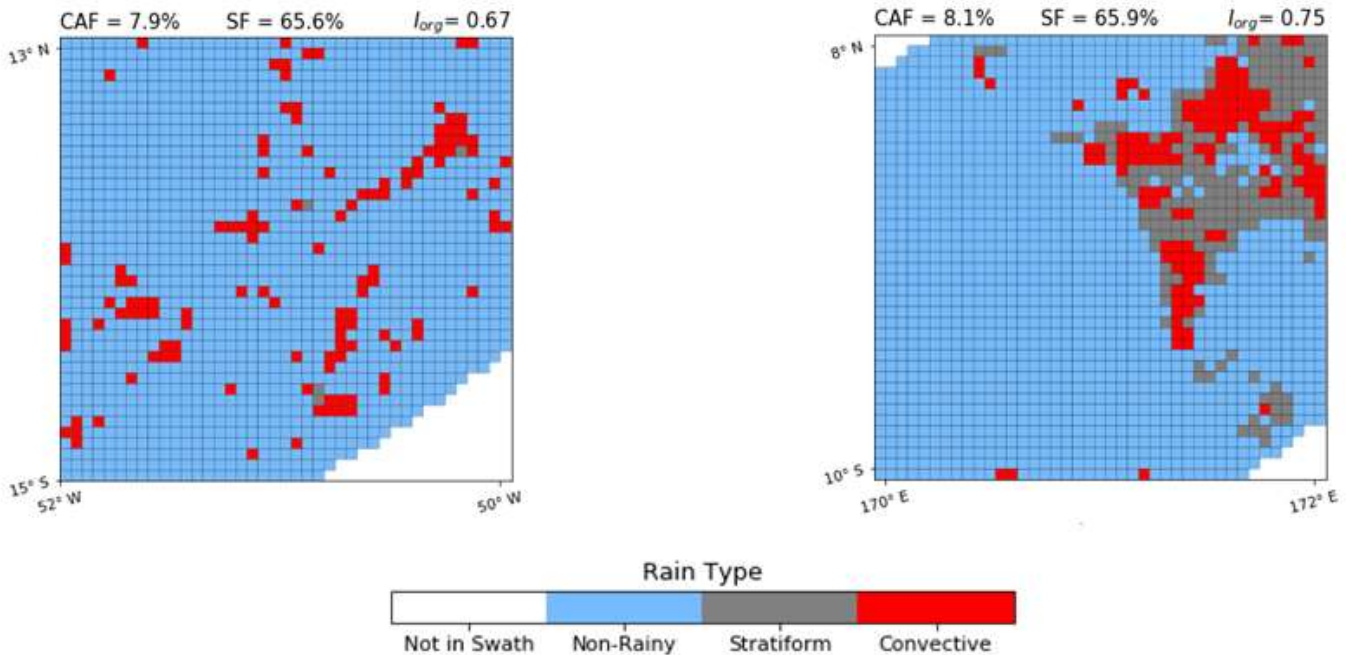


Figure 2.4: Example of a scene with (left) relatively low I_{org} and (right) relatively high I_{org} . The right panel has more convective pixels with small NNDs as opposed to the left panel, which has more isolated convective pixels far from their nearest neighbor.

$$I_{org} = \sum_{i=1}^N \left(\frac{m_i}{N} \right) (NNCDF_{ran}(r_{i+1}) - NNCDF_{ran}(r_i)), \quad (2.2)$$

where r_i is the i^{th} NND (sorted as before), m_i is the number of convective pixels with $\text{NND} < r_i$, and where we have formally taken $r_{N+1} = \infty$ so that $NNCDF_{ran}(r_{N+1}) = 1$. For every scene, we compute I_{org} using Eq. 2.2. This number characterizes the degree of convective organization exhibited by the convective pixels in the scene.

2.2.2 Isolating Mesoscale Convective Organization

Tropical precipitation is affected by an innumerable suite of variables. To quantify the effects of mesoscale convective organization on tropical precipitation, we will stratify our data to compare scenes that differ in their degree of convective organization, but which are similar otherwise, especially with respect to variables that strongly control precipitation intensity. Given our stated interest in aiding efforts to incorporate representations of mesoscale convective organization into operational GCMs, we stratify scenes by two quantities that have been shown to strongly control tropical precipitation intensity, while simultaneously being feasible for a GCM to compute. These two quantities are convective area fraction (CAF) and saturation fraction (SF).

CAF will be computed for each scene by dividing the area covered by the scene's convective pixels by the total area of the scene. This quantity has been shown to strongly control precipitation intensity (Doneaud et al., 1984; Nuijens et al., 2009; Davies et al., 2013; Brueck et al., 2020). By binning our data so as to compare scenes with similar CAF, we will avoid the effects noted in Semie and Bony (2020), whereby precipitation over domains with organized convection is affected by the large non-convective, non-rainy region incurred by the aggregation of convection.

SF is computed using ERA5 vertical profiles of specific humidity (q) and temperature. For each scene, the ERA5 data is co-located and linearly interpolated to provide a best estimate of vertical temperature and moisture profiles over the scene. Using the approximation for saturation vapor pressure given in Bolton (1980), saturation vapor pressure (q^*) is computed for each pressure level between 1000 hPa and 100 hPa, with 100 hPa increments. The saturation fraction of the scene is thus given by

$$SF = \frac{\langle q \rangle}{\langle q^* \rangle}$$

where $\langle \cdot \rangle$ indicates vertical integration from 1000 hPa to 100 hPa and areal integration over the scene's area. That is, SF is given by the total water vapor present over the domain, normalized by the water vapor that would be present in the domain if every column were saturated. This quantity has also been shown to strongly control precipitation, with precipitation increasing nonlinearly with SF beyond a certain “pickup point” of $\sim 70\%$ (Bretherton et al., 2004; Ahmed and Schumacher, 2015; Rushley et al., 2018; Wolding et al., 2020; Adames et al., 2021).

Chapter 3. RESULTS AND DISCUSSION

In this chapter we state our findings. We examined the role of mesoscale convective organization in modulating of tropical precipitation intensity. We also examined how this modulation differentially impacts convective and stratiform precipitation.

3.1 THE ENHANCEMENT OF TROPICAL PRECIPITATION INTENSITY

To isolate the effects of mesoscale convective organization, we binned our scenes by their CAF and SF. The mean precipitation intensity for each CAF and SF bin considered is shown in Fig. 3.1. We can see that precipitation intensity does indeed increase with CAF and with SF, as expected from previous studies. If we examine the bin-mean value of I_{org} in this space (Fig. 3.2), we see that I_{org} exhibits a monotonic decrease with CAF, and to a lesser extent a decrease with SF. This finding is in fact consistent with the findings of Semie and Bony (2020) and Brueck et al. (2020).

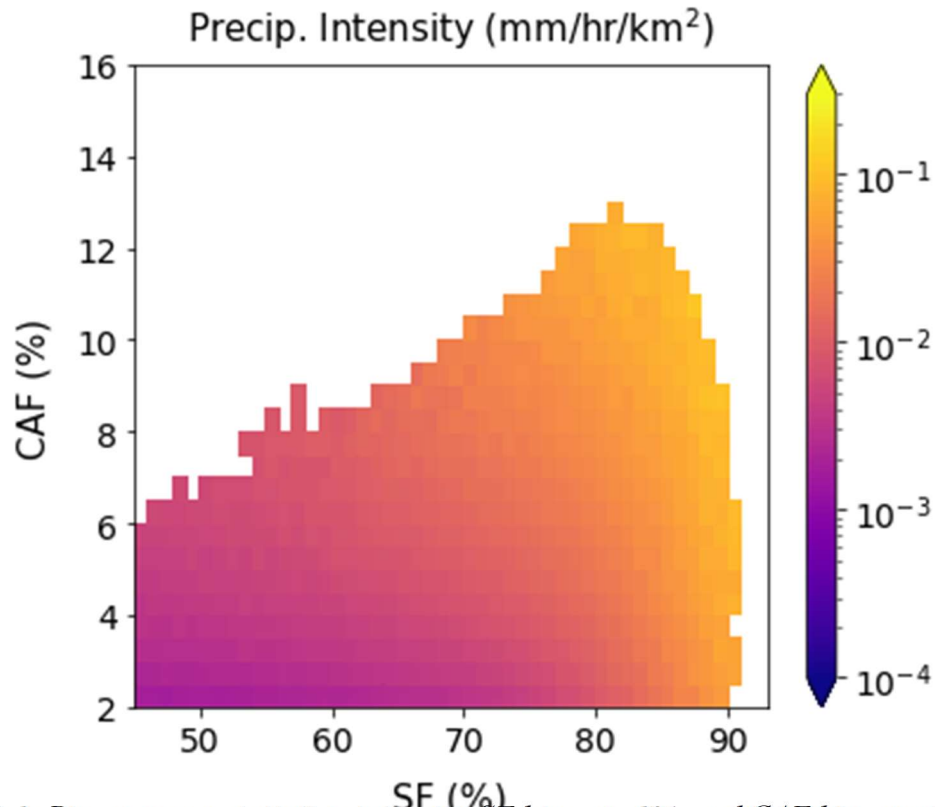


Figure 3.1: Bin-mean precipitation intensity. SF bins are 1%, and CAF bins are 0.5%.

These studies concluded that precipitation intensity is not affected by convective organization, and that precipitation intensity may even be suppressed by a stronger degree of convective organization. However, our approach to investigating the role of convective organization in modulating precipitation intensity is distinct from these studies; we will only compare scenes that have equal (or near-equal) CAF and SF, but differing values of I_{org} . This will allow for fairer comparisons between scenes and will allow the effects of mesoscale convective organization to be isolated from other factors that affect precipitation rate.

To quantify the effect of mesoscale convective organization on precipitation intensity, for each CAF-SF bin we sort all scenes that fall within that bin by their I_{org} value. We take the scenes whose I_{org} values fall within the top quartile of values as the “strongly organized” scenes for that bin; similarly, those scenes with I_{org} values in the bottom quartile are considered the “weakly organized” scenes. Using quartiles to distinguish strongly and weakly organized scenes is an arbitrary choice, and primarily a matter of convenience. The main results presented in this section

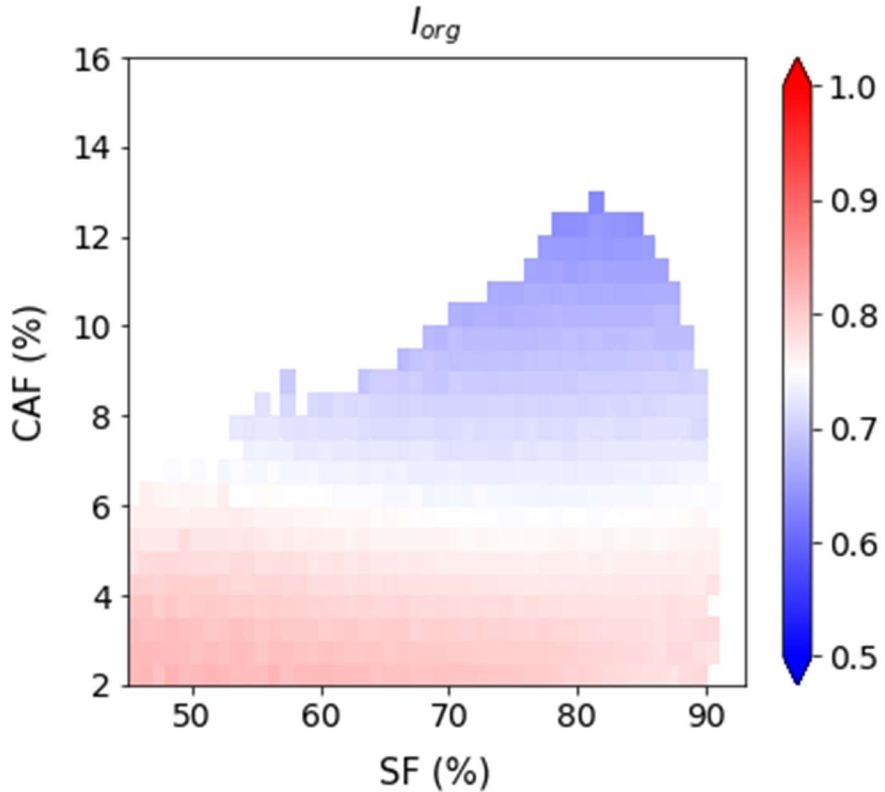


Figure 3.2: Bin mean values of I_{org} . We note that there is a monotonic decrease with CAF.

are largely the same if other percentile ranges are chosen. For every bin, the mean precipitation intensity of the strongly organized and weakly organized scenes is computed; these mean intensities will be labelled P^{Strong} and P^{Weak} , respectively. We then define the “*precipitation enhancement due to mesoscale convective organization*”, or PEMC, as the percent difference between P^{Strong} and P^{Weak} :

$$\text{PEMC} = \frac{P^{Strong} - P^{Weak}}{P^{Weak}} \times 100\% \quad (3.1)$$

To determine the statistical significance of the difference between P^{Strong} and P^{Weak} , a Monte Carlo test is performed, where the scenes are randomly sorted, and the absolute difference between the mean precipitation intensities of the first quarter and fourth quarter of scenes is compared against the absolute difference between P^{Strong} and P^{Weak} . This test is performed 1000 times for each bin. The fraction of random configurations that produce a greater difference in mean

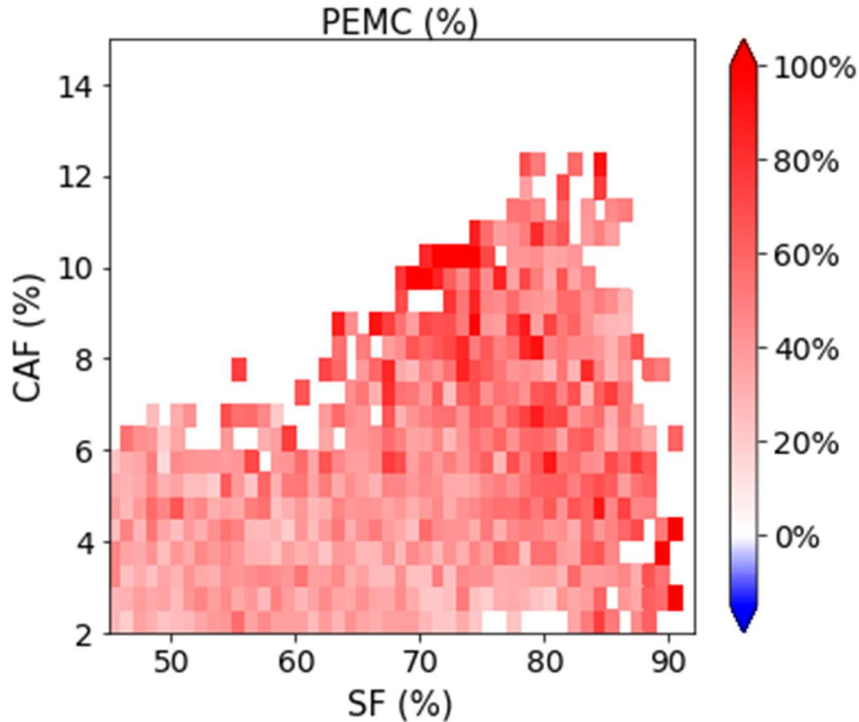


Figure 3.3: PEMC values for CAF-SF bins with a statistically significant difference of precipitation intensities between strongly and weakly organized scenes. The mean PEMC value is 47.01%

precipitation intensities between first and fourth quarters is taken as the p-value of the difference. Bins with a p-value less than 0.05 (95th confidence interval) are taken to be statistically significant.

The statistically significant values of PEMC for each bin are shown in Fig. 3.3. Of immediate note is the fact that all statistically significant values are positive. This indicates that there is a robust increase in precipitation intensity associated with a greater I_{org} value when CAF and SF are prescribed. Since we have defined the strongly and weakly organized scenes for each CAF-SF bin, the variance of I_{org} with CAF shown in Fig. 3.2 is controlled for by this method. The mean statistically significant value of PEMC is 47.01%. This number serves as an estimate of the enhancement of precipitation intensity that can be associated with a stronger degree of convective organization, controlling for other factors. In other words, among scenes with equal SF and CAF, those whose convective pixels are more spatially clustered, as quantified by I_{org} , undergo on

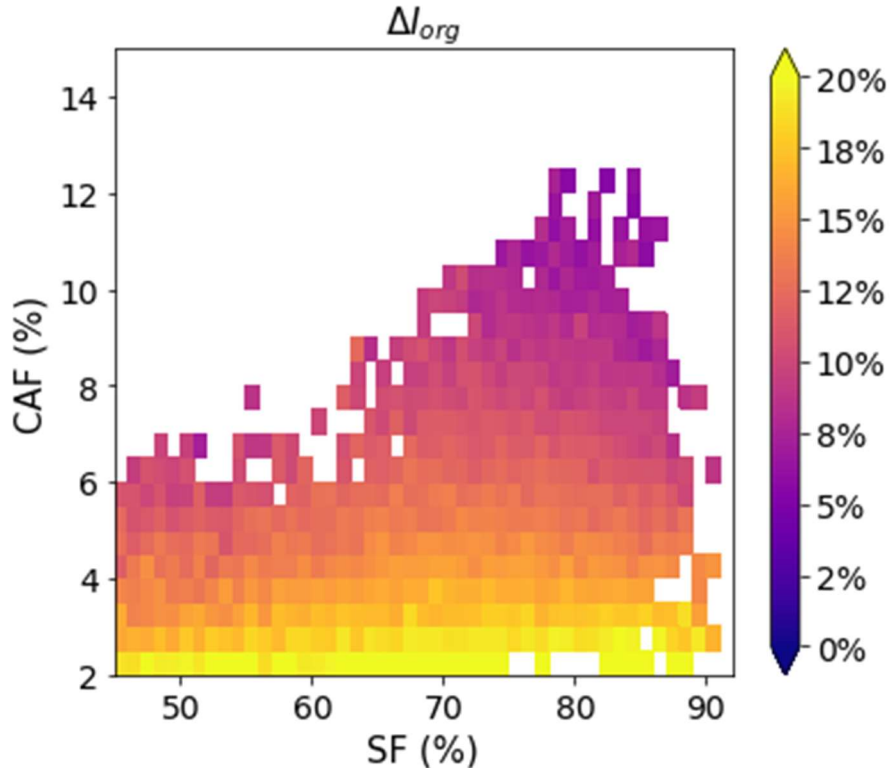


Figure 3.4: The fractional increase in mean value of I_{org} between weakly and strongly clustered scenes for bins with statistically significant precipitation enhancements. This fractional change in I_{org} decreases with CAF, suggesting that the sensitivity of precipitation intensity to the degree of mesoscale convective clustering is dependent on the number of convective entities present.

average 47.01% more intense precipitation than those scenes whose convective pixels are weakly organized. This value also serves to quantify the variance in precipitation intensity that is missing from numerical modelling frameworks that do not represent mesoscale convective organization in some way.

We performed a similar analysis by computing the fractional difference in mean I_{org} values for each bin; that is, we compute the percent difference in mean I_{org} values of strongly and weakly organized scenes for each CAF-SF bin. This is shown in Fig. 3.4. We can see that this difference decreases with CAF, similar to I_{org} 's dependence on CAF shown in Fig. 3.2. This suggests that the enhancement of precipitation that we attribute to a stronger degree of mesoscale convective organization is mediated by mutual interactions between cumuli. Scenes with a larger number of convective pixels, and thus more convection, can experience as large a fractional enhancement of precipitation intensity with a smaller change to the degree of convective organization of the scene.

3.2 CONVECTIVE AND STRATIFORM COMPONENTS OF ENHANCEMENT.

To examine how a stronger degree of mesoscale convective organization differentially affects convective and stratiform processes, we first must decompose PEMC into stratiform and convective components. We can decompose a scene's precipitation field as

$$P = (P_{conv} \times \text{CAF}) + (P_{strat} \times \text{SAF})$$

where P_{conv} and P_{strat} are the conditional convective and stratiform precipitation intensities, respectively, and CAF and SAF are the convective and stratiform area fractions, respectively. The SAF is computed in an analogous manner to CAF; the ratio of stratiform pixel area to total scene area. We can use this decomposition to express P^{Weak} as

$$P^{Weak} = P_{conv}^{Weak} \times \text{CAF}^{Weak} + P_{strat}^{Weak} \times \text{SAF}^{Weak} \quad (3.2)$$

where the terms are all mean values of the indicated quantity among weakly organized scenes. We can further express P^{Strong} in a similar form as Eq. 3.2, but in terms of the mean values of weakly organized scenes:

$$P^{Strong} = (P_{conv}^{Weak} + \Delta P_{conv})(CAF^{Weak} + \Delta CAF) + (P_{strat}^{Weak} + \Delta P_{strat})(SAF^{Weak} + \Delta SAF),$$

where Δx indicates the difference in the mean value of x between strongly and weakly organized scenes (i.e., $\Delta P_{conv} = P_{conv}^{Strong} - P_{conv}^{Weak}$). We note that since the strongly and weakly organized scenes come from the same CAF bin, we can take $\Delta CAF \approx 0$. Expanding this equation and subtracting Eq. 3.2. yields an expression for $\Delta P = P^{Strong} - P^{Weak}$:

$$\Delta P = (CAF \times \Delta P_{conv}) + (SAF^{Weak} \times \Delta P_{strat}) + (P_{strat}^{Weak} \times \Delta SAF) + (\Delta P_{strat} \times \Delta SAF) \quad (3.3)$$

From Eq. 3.3 we can see that the enhancement of precipitation associated with a stronger degree of convective organization can be decomposed into four terms: a strengthening of convective precipitation intensity, a strengthening of stratiform precipitation intensity, an increase in stratiform area fraction, and a covariance term associated with changes in stratiform precipitation intensity and area fraction.

Using the fact that $PEMC = \Delta P / P^{Weak}$, and using Eq. 3.3, we computed each parenthetical term for each CAF-SF bin as a component of PEMC. The results are shown in Fig. 3.3. We can see that, for $SF < 70\%$, the dominant contribution to PEMC is from an enhancement of convective precipitation rate. This indicates that when the environment is less than 70% saturated, the enhancement of precipitation associated with a stronger degree of convective organization is primarily attributable to an enhanced convective precipitation intensity. However, for $SF > 70\%$, the enhancement of stratiform area fraction becomes of increasingly large importance the higher the saturation fraction of the environment. This transition can be seen more clearly by considering the mean contribution to PEMC (fraction of PEMC) by the convective component (first parenthetical term in Eq. 3.3) and the stratiform component (sum of the latter three parenthetical terms of Eq. 3.3), averaged over CAF bins. This is shown in Fig. 3.5, where we can see that the convective component is the dominant component of PEMC for $SF < 70\%$; for SF in between 70% and 85%, the stratiform and convective contributions are comparable in magnitude; and for $SF > 85\%$, it is in fact the stratiform component that is the dominant component of PEMC. This implies that, as the environment becomes increasingly saturated, the relevance of stratiform

processes to the enhancement of precipitation associated with an increase in degree of convective organization increases.

This transition of PEMC as being dominated by an enhancement of convective precipitation intensity is reminiscent of the fact that the prevalence of stratiform precipitation also increases with SF (Ahmed and Schumacher, 2015; Wolding et al., 2020). Fig. 3.4 also shows the mean convective rain fraction (CRF) and stratiform rain fraction (CRF), averaged over CAF bins. We can see that, to first order, the relative importance of the stratiform or convective component of PEMC at a given SF tracks strongly with the relative abundance of the associated precipitation

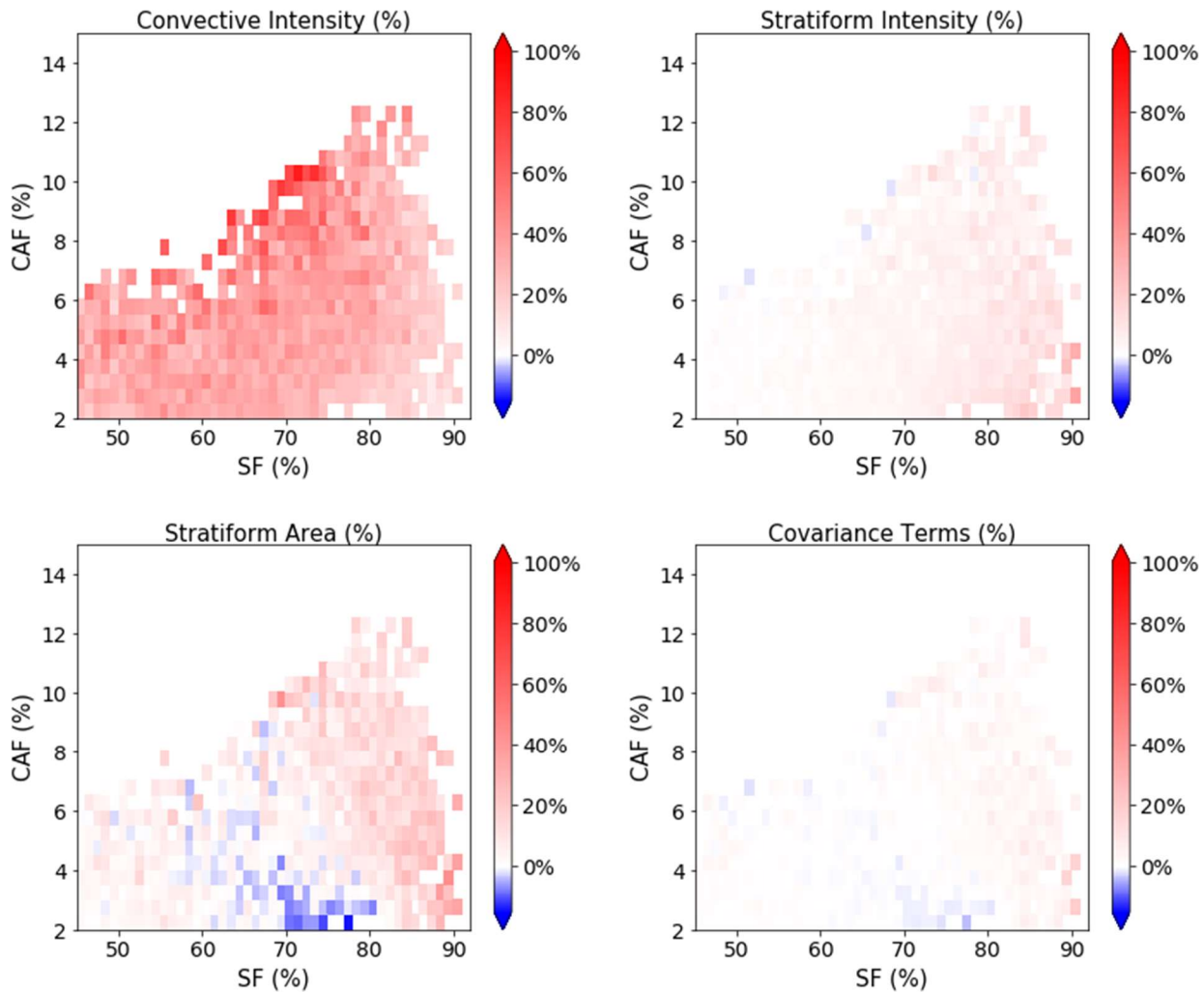


Figure 3.4: The enhancement of precipitation attributed to (top left) strengthened convective precipitation intensity, (top right) strengthened stratiform precipitation intensity, (bottom left) larger stratiform area fraction, and (bottom right) covariance between stratiform area fraction and stratiform precipitation intensity. Each component is computed using Eq. 3.3.

type at that SF. This suggests that, for a given SF, the relative importance of PEMC's convective and stratiform components are set by the relative frequency of convective and stratiform precipitation at that SF. That is, at a given SF, the fraction of total precipitation that is convective or stratiform is largely determined by the SF of the environment; mesoscale convective clustering increases the total amount of precipitation but does not substantially alter the partition between convective and stratiform precipitation.

To verify this hypothesized invariance of the convective/stratiform partition, we compared the CRF and SRF of strongly and weakly organized scenes, averaged over each CAF bin with a statistically significant value of PEMC. As shown in Fig. 3.5, both CRF and SRF differ only marginally between strongly and weakly organized scenes. This indicates that, to first order, mesoscale convective clustering does not significantly alter the partition between convective and

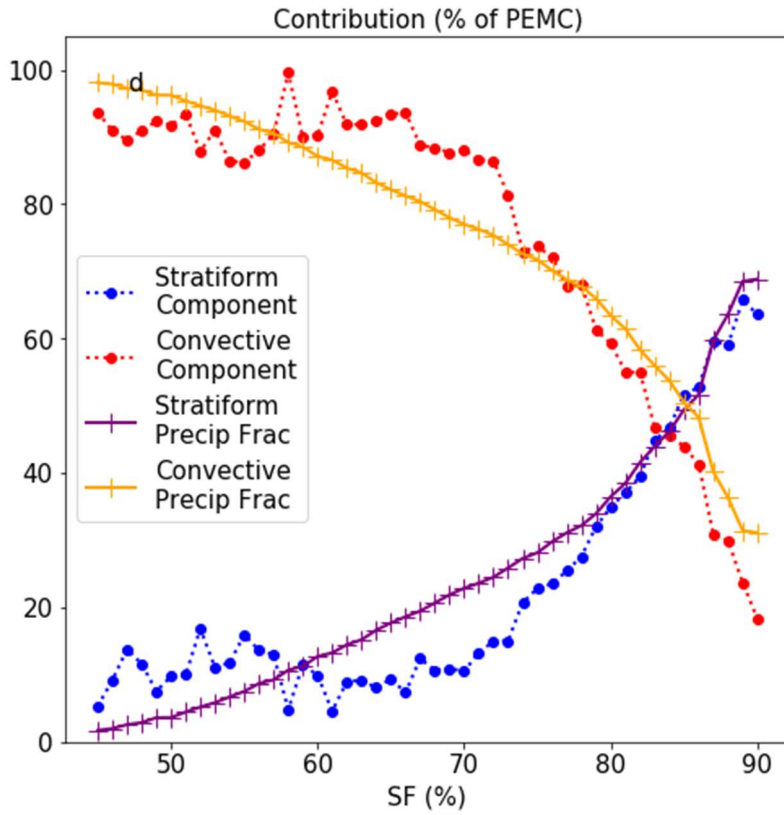


Figure 3.5: Average contribution of convective and stratiform components of PEMC. Also shown are mean convective and stratiform rain fractions. We observe that the convective and stratiform contributions to PEMC are strongly correlated with the convective and stratiform rain fractions, respectively.

stratiform elements. We do note that there is a slight, but non-negligible, difference in the CRF and SRF between strongly and weakly organized scenes in the range $60\% < SF < 80\%$. In this range, strongly organized scenes have a larger CRF (and, consequently, smaller SRF) than weakly organized scenes. Since CAF is constrained, this indicates that in this range, the convection that exists is more intense. This can be understood as a consequence of the way that cumuli interact with their environment, and with one another, via entrainment and detrainment. Several studies

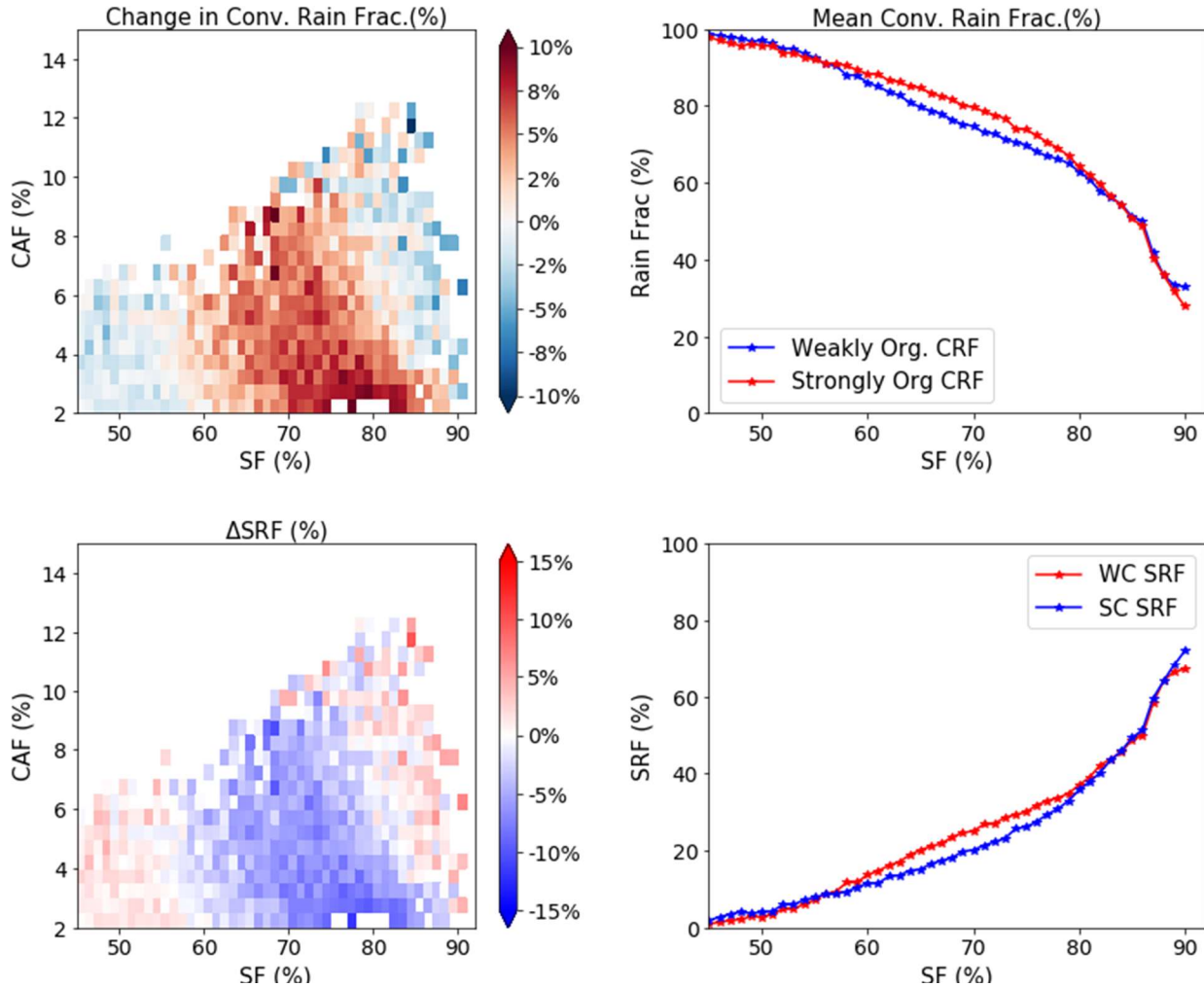


Figure 3.6: Change in (top left) convective and (bottom left) stratiform rain fractions between strongly and weakly organized scenes. The average change over CAF bins is shown in the right panel (top convective, bottom stratiform)s. The difference between the CRF of strongly and weakly clustered is small, with a mean difference in CRF of 3.3%. The difference between the two is greatest in the range $60\% < SF < 80\%$.

have suggested that organized convection is able to form a “moist shield” around themselves, and thus creating, via detrainment of water into the non-cloudy environment, a region of relatively moist air around the spatially clustered cumuli (Becker et al., 2018; Feng et al., 2015; Hannah, 2017; Moser and Lasher-Trapp, 2018). This allows for the organized cumuli to entrain air that is potentially moister than the environment, mitigating the reduction of buoyancy caused by the entrainment of subsaturated, environmental air. From this conceptual framework, the fact that convection is most strongly affected in the range $60\% < SF < 80\%$ is because for SF values that are too small (less than 60%), the salubrious effects of convective organization on the strength of convection are mitigated by the large subsaturation of the air. Scenes with $SF < 60\%$ are too dry for deep convection to survive for long; as such, even organized convection cannot substantially impact the strength of convection. In the case of scenes with $SF > 80\%$, a mirror phenomenon occurs: since the environment is so close to saturation, the protective barrier formed by the “moist shell” of organized convection is, in a sense, superfluous to the convection. Thus, convective strength is less strongly affected at high SF. This argument is essentially a post-hoc interpretation of our results, and cannot be strongly supported by the results shown here. However, demonstrated dependence of stratiform and convective components of organization-driven enhancement on SF suggests the value in further pursuing this idea to obtain a better understanding of the dynamical reasons for this dependence.

Chapter 4. CONCLUSIONS

In this thesis, we have obtained a quantitative estimate of the enhancement of tropical precipitation intensity associated with a stronger degree of mesoscale convective organization. We have found that, when SF and CAF are prescribed, scenes whose constituent convective elements are more strongly organized experience an average of 47.01% more intense precipitation than scenes with less strongly organized convection. This finding is intended to serve as an observational benchmark against which parametrizations and model representations of mesoscale convective organization, and its effects on precipitation, can be evaluated. We have also shown that the nature of this enhancement depends on how saturated the environment is. When the environment is less than 70% saturated, the enhanced precipitation ascribable to a stronger degree of convective organization is primarily caused by an increase in convective precipitation intensity. When the environment is more than 70% saturated, however, the enhancement of precipitation is due both to an increased convective precipitation enhancement as well as an increase in stratiform area fraction. It is found that this transition is a consequence of the fact that mesoscale convective organization, to first order, does not affect the partition between convective and stratiform precipitation. That partition is primarily affected by the SF of the scene; strongly organized scenes precipitate more intensely than weakly organized scenes while still exhibiting near-equal convective and stratiform rain fractions. Despite this near-invariance of convective and stratiform rain fractions with an increase in degree of convective organization, it is found that mesoscale convective organization most strongly affects convection when SF is in the range $60\% < \text{SF} < 80\%$. It is argued that this is because, in this range, the environment is moist enough to allow deep convection to exist, while also not being so moist as to render the salubrious effects of convective organization moot.

This work offers several potential avenues for further inquiry. These results can be compared against the outputs of global storm-permitting models, such as DYAMOND (Stevens et al., 2019). Doing so will test the efficacy of these models, and whether convective organization can be represented in models with sufficiently high resolution. This work also serves as further evidence of the interconnectedness of convective and stratiform processes. While often considered distinct, both in conceptual models and numerical schemes, convection and stratiform clouds are

intimately linked. This work thus serves as further evidence of the importance of pursuing a unified, quantitative approach to modelling clouds of all types (Arakawa, 2004).

Chapter 5. REFERENCES

- Adames, Á.F., Powell, S.W., Ahmed, F., Mayta, V.C., Neelin, J.D., 2021. Tropical Precipitation Evolution in a Buoyancy-Budget Framework. *Journal of the Atmospheric Sciences* 78, 509–528. <https://doi.org/10.1175/JAS-D-20-0074.1>
- Ahmed, F., Schumacher, C., 2015. Convective and Stratiform Components of the Precipitation-Moisture Relationship. *Geophysical Research Letters* 42, 10,453-10,462. <https://doi.org/10.1002/2015GL066957>
- Arakawa, A., 2004. The Cumulus Parameterization Problem: Past, Present, and Future. *JOURNAL OF CLIMATE* 17, 33.
- Awaka, J., Iguchi, T., Okamoto, K., 2009. TRMM PR Standard Algorithm 2A23 and its Performance on Bright Band Detection. *Journal of the Meteorological Society of Japan* 87A, 31–52. <https://doi.org/10.2151/jmsj.87A.31>
- Becker, T., Bretherton, C.S., Hohenegger, C., Stevens, B., 2018. Estimating Bulk Entrainment with Unaggregated and Aggregated Convection: Organization's Effect on Entrainment. *Geophys. Res. Lett.* 45, 455–462. <https://doi.org/10.1002/2017GL076640>
- Bolton, D., 1980. The Computation of Equivalent Potential Temperature. *Monthly Weather Review* 108, 1046–1053. [https://doi.org/10.1175/1520-0493\(1980\)108<1046:TCOEPT>2.0.CO;2](https://doi.org/10.1175/1520-0493(1980)108<1046:TCOEPT>2.0.CO;2)
- Bretherton, C.S., Peters, M.E., Back, L.E., 2004. Relationships between Water Vapor Path and Precipitation over the Tropical Oceans. *Journal of Climate* 17, 1517–1528. [https://doi.org/10.1175/1520-0442\(2004\)017<1517:RBWVPA>2.0.CO;2](https://doi.org/10.1175/1520-0442(2004)017<1517:RBWVPA>2.0.CO;2)
- Brueck, M., Hohenegger, C., Stevens, B., 2020. Mesoscale Marine Tropical Precipitation Varies Independently from the Spatial Arrangement of Its Convective Cells. *Q.J.R. Meteorol. Soc* 146, 1391–1402. <https://doi.org/10.1002/qj.3742>
- Cheng, C.-P., Houze, R.A., 1979. The Distribution of Convective and Mesoscale Precipitation in GATE Radar Echo Patterns. *Monthly Weather Review* 107, 1370–1381. [https://doi.org/10.1175/1520-0493\(1979\)107<1370:TDOCAM>2.0.CO;2](https://doi.org/10.1175/1520-0493(1979)107<1370:TDOCAM>2.0.CO;2)
- Cheng, W., Kim, D., Rowe, A., 2018. Objective Quantification of Convective Clustering Observed During the AMIE/DYNAMO Two-Day Rain Episodes. *J. Geophys. Res. Atmos.* 123. <https://doi.org/10.1029/2018JD028497>
- Davies, L., Jakob, C., May, P., Kumar, V.V., Xie, S., 2013. Relationships Between the Large-Scale Atmosphere and the Small-Scale Convective State for Darwin, Australia: Relationships Between Scales at Darwin. *J. Geophys. Res. Atmos.* 118, 11,534-11,545. <https://doi.org/10.1002/jgrd.50645>
- Doneaud, A., Ionescu-Niscov, S., Priegnitz, D.L., Smith, P.L., 1984. The Area-Time Integral as an Indicator for Convective Rain Volumes. *Journal of Applied Meteorology and Climatology* 23, 555–561. [https://doi.org/10.1175/1520-0450\(1984\)023<0555:TATIAA>2.0.CO;2](https://doi.org/10.1175/1520-0450(1984)023<0555:TATIAA>2.0.CO;2)
- Donner, L.J., 1993. A Cumulus Parameterization Including Mass Fluxes, Vertical Momentum Dynamics, and Mesoscale Effects. *Journal of the Atmospheric Sciences* 50, 889–906. [https://doi.org/10.1175/1520-0469\(1993\)050<0889:ACPIMF>2.0.CO;2](https://doi.org/10.1175/1520-0469(1993)050<0889:ACPIMF>2.0.CO;2)
- Feng, Z., Hagos, S., Rowe, A.K., Burleyson, C.D., Martini, M.N., Szoéke, S.P., 2015. Mechanisms of Convective Cloud Organization by Cold Pools Over Tropical Warm

- Ocean During the AMIE/DYNAMO Field Campaign. *J. Adv. Model. Earth Syst.* 7, 357–381. <https://doi.org/10.1002/2014MS000384>
- Hannah, W.M., 2017. Entrainment versus Dilution in Tropical Deep Convection. *Journal of the Atmospheric Sciences* 74, 3725–3747. <https://doi.org/10.1175/JAS-D-16-0169.1>
- Hersbach, H., Bell, B., Berrisford, P., Biavati, G., Horányi, A., Muñoz Sabater, J., Nicolas, J., Peubey, C., Radu, R., Rozum, I., Schepers, D., Simmons, A., Soci, D., Dee, D., Thépaut, J.-N., 2020. ERA5 Hourly Data on Single Levels from 1979 to Present.
- Houze, R.A., 2004. Mesoscale convective systems. *Reviews of Geophysics* 42. <https://doi.org/10.1029/2004RG000150>
- Houze, R.A., 1997. Stratiform Precipitation in Regions of Convection: A Meteorological Paradox? *Bulletin of the American Meteorological Society* 78, 2179–2196. [https://doi.org/10.1175/1520-0477\(1997\)078<2179:SPIROC>2.0.CO;2](https://doi.org/10.1175/1520-0477(1997)078<2179:SPIROC>2.0.CO;2)
- Iguchi, T., Meneghini, R., 1994. Intercomparison of Single-Frequency Methods for Retrieving a Vertical Rain Profile from Airborne or Spaceborne Radar Data. *Journal of Atmospheric and Oceanic Technology* 11, 1507–1516. [https://doi.org/10.1175/1520-0426\(1994\)011<1507:IOSFMF>2.0.CO;2](https://doi.org/10.1175/1520-0426(1994)011<1507:IOSFMF>2.0.CO;2)
- Jaramillo, L., Poveda, G., Mejía, J.F., 2017. Mesoscale Convective Systems and Other Precipitation Features Over the Tropical Americas and Surrounding Seas as Seen by TRMM. *International Journal of Climatology* 37, 380–397. <https://doi.org/10.1002/joc.5009>
- Khouider, B., Moncrieff, M.W., 2015. Organized Convection Parameterization for the ITCZ*. *Journal of the Atmospheric Sciences* 72, 3073–3096. <https://doi.org/10.1175/JAS-D-15-0006.1>
- Kiladis, G.N., Wheeler, M.C., Haertel, P.T., Straub, K.H., Roundy, P.E., 2009. Convectively coupled equatorial waves. *Reviews of Geophysics* 47. <https://doi.org/10.1029/2008RG000266>
- Leary, C.A., 1984. Precipitation Structure of the Cloud Clusters in a Tropical Easterly Wave. *Monthly Weather Review* 112, 313–325. [https://doi.org/10.1175/1520-0493\(1984\)112<0313:PSOTCC>2.0.CO;2](https://doi.org/10.1175/1520-0493(1984)112<0313:PSOTCC>2.0.CO;2)
- Madden, R.A., Julian, P.R., 1972. Description of Global-Scale Circulation Cells in the Tropics with a 40–50 Day Period. *Journal of the Atmospheric Sciences* 29, 1109–1123. [https://doi.org/10.1175/1520-0469\(1972\)029<1109:DOGSAC>2.0.CO;2](https://doi.org/10.1175/1520-0469(1972)029<1109:DOGSAC>2.0.CO;2)
- Madden, R.A., Julian, P.R., 1971. Detection of a 40–50 Day Oscillation in the Zonal Wind in the Tropical Pacific. *Journal of the Atmospheric Sciences* 28, 702–708. [https://doi.org/10.1175/1520-0469\(1971\)028<0702:DOADOI>2.0.CO;2](https://doi.org/10.1175/1520-0469(1971)028<0702:DOADOI>2.0.CO;2)
- Majda, A.J., Biello, J.A., 2004. A multiscale model for tropical intraseasonal oscillations. *Proceedings of the National Academy of Sciences* 101, 4736–4741. <https://doi.org/10.1073/pnas.0401034101>
- Mapes, B., Neale, R., 2011. Parameterizing Convective Organization to Escape the Entrainment Dilemma: Parameterizing Convective Organization. *J. Adv. Model. Earth Syst.* 3, n/a-n/a. <https://doi.org/10.1029/2011MS000042>
- Mapes, B., Tulich, S., Lin, J., Zuidema, P., 2006. The Mesoscale Convection Life Cycle: Building Block or Prototype for Large-Scale Tropical Waves? *Dynamics of Atmospheres and Oceans* 42, 3–29. <https://doi.org/10.1016/j.dynatmoce.2006.03.003>

- Meehl, G.A., Lukas, R., Kiladis, G.N., Weickmann, K.M., Matthews, A.J., Wheeler, M., 2001. A conceptual framework for time and space scale interactions in the climate system. *Climate Dynamics* 17, 753–775. <https://doi.org/10.1007/s003820000143>
- Moncrieff, M.W., 2019. Toward a Dynamical Foundation for Organized Convection Parameterization in GCMs. *Geophysical Research Letters* 46, 14103–14108. <https://doi.org/10.1029/2019GL085316>
- Moncrieff, M.W., 2004. Analytic Representation of the Large-Scale Organization of Tropical Convection. *JOURNAL OF THE ATMOSPHERIC SCIENCES* 61, 18.
- Moncrieff, M.W., Liu, C., Bogenschutz, P., 2017. Simulation, Modeling, and Dynamically Based Parameterization of Organized Tropical Convection for Global Climate Models. *Journal of the Atmospheric Sciences* 74, 1363–1380. <https://doi.org/10.1175/JAS-D-16-0166.1>
- Moser, D.H., Lasher-Trapp, S., 2018. Cloud-Spacing Effects upon Entrainment and Rainfall along a Convective Line. *Journal of Applied Meteorology and Climatology* 57, 1865–1882. <https://doi.org/10.1175/JAMC-D-17-0363.1>
- Nakazawa, T., 1988. Tropical Super Clusters within Intraseasonal Variations over the Western Pacific. *Journal of the Meteorological Society of Japan. Ser. II* 66, 823–839. https://doi.org/10.2151/jmsj1965.66.6_823
- Nesbitt, S.W., Cifelli, R., Rutledge, S.A., 2006. Storm Morphology and Rainfall Characteristics of TRMM Precipitation Features. *Monthly Weather Review* 134, 2702–2721. <https://doi.org/10.1175/MWR3200.1>
- Nuijens, L., Stevens, B., Siebesma, A.P., 2009. The Environment of Precipitating Shallow Cumulus Convection. *Journal of the Atmospheric Sciences* 66, 1962–1979. <https://doi.org/10.1175/2008JAS2841.1>
- Park, S., 2014. A Unified Convection Scheme (UNICON). Part I: Formulation. *Journal of the Atmospheric Sciences* 71, 3902–3930. <https://doi.org/10.1175/JAS-D-13-0233.1>
- Rio, C., Del Genio, A.D., Hourdin, F., 2019. Ongoing Breakthroughs in Convective Parameterization. *Curr Clim Change Rep* 5, 95–111. <https://doi.org/10.1007/s40641-019-00127-w>
- Roca, R., Aublanc, J., Chambon, P., Fiolleau, T., Viltard, N., 2014. Robust Observational Quantification of the Contribution of Mesoscale Convective Systems to Rainfall in the Tropics. *Journal of Climate* 27, 4952–4958. <https://doi.org/10.1175/JCLI-D-13-00628.1>
- Rushley, S.S., Kim, D., Bretherton, C.S., Ahn, M. -S., 2018. Reexamining the Nonlinear Moisture-Precipitation Relationship Over the Tropical Oceans. *Geophys. Res. Lett.* 45, 1133–1140. <https://doi.org/10.1002/2017GL076296>
- Rutledge, S.A., Houze, R.A., 1987. A Diagnostic Modelling Study of the Trailing Stratiform Region of a Midlatitude Squall Line. *Journal of the Atmospheric Sciences* 44, 2640–2656. [https://doi.org/10.1175/1520-0469\(1987\)044<2640:ADMSOT>2.0.CO;2](https://doi.org/10.1175/1520-0469(1987)044<2640:ADMSOT>2.0.CO;2)
- Schumacher, C., Houze, R.A., 2003. Stratiform Rain in the Tropics as Seen by the TRMM Precipitation Radar. *Journal of Climate* 16, 1739–1756. [https://doi.org/10.1175/1520-0442\(2003\)016<1739:SRITTA>2.0.CO;2](https://doi.org/10.1175/1520-0442(2003)016<1739:SRITTA>2.0.CO;2)
- Semie, A.G., Bony, S., 2020. Relationship Between Precipitation Extremes and Convective Organization Inferred from Satellite Observations. *Geophys. Res. Lett.* 47. <https://doi.org/10.1029/2019GL086927>
- Stein, T.H.M., Holloway, C.E., Tobin, I., Bony, S., 2017. Observed Relationships between Cloud Vertical Structure and Convective Aggregation over Tropical Ocean. *Journal of Climate* 30, 2187–2207. <https://doi.org/10.1175/JCLI-D-16-0125.1>

- Steiner, M., Houze, R.A., Yuter, S.E., 1995. Climatological Characterization of Three-Dimensional Storm Structure from Operational Radar and Rain Gauge Data. *Journal of Applied Meteorology and Climatology* 34, 1978–2007. [https://doi.org/10.1175/1520-0450\(1995\)034<1978:CCOTDS>2.0.CO;2](https://doi.org/10.1175/1520-0450(1995)034<1978:CCOTDS>2.0.CO;2)
- Stevens, B., Satoh, M., Auger, L., Biercamp, J., Bretherton, C.S., Chen, X., Düben, P., Judt, F., Khairoutdinov, M., Klocke, D., Kodama, C., Kornblueh, L., Lin, S.-J., Neumann, P., Putman, W.M., Röber, N., Shibuya, R., Vanniere, B., Vidale, P.L., Wedi, N., Zhou, L., 2019. DYAMOND: the DYnamics of the Atmospheric general circulation Modeled On Non-hydrostatic Domains. *Progress in Earth and Planetary Science* 6, 61. <https://doi.org/10.1186/s40645-019-0304-z>
- Tan, J., Jakob, C., Rossow, W.B., Tselioudis, G., 2015. Increases in Tropical Rainfall Driven by Changes in Frequency of Organized Deep Convection. *Nature* 519, 451–454. <https://doi.org/10.1038/nature14339>
- Tobin, I., Bony, S., Roca, R., 2012. Observational Evidence for Relationships between the Degree of Aggregation of Deep Convection, Water Vapor, Surface Fluxes, and Radiation. *Journal of Climate* 25, 6885–6904. <https://doi.org/10.1175/JCLI-D-11-00258.1>
- Tompkins, A.M., Semie, A.G., 2017. Organization of Tropical Convection in Low Vertical Wind Shears: Role of Updraft Entrainment. *J. Adv. Model. Earth Syst.* 9, 1046–1068. <https://doi.org/10.1002/2016MS000802>
- Wolding, B., Dias, J., Kiladis, G., Ahmed, F., Powell, S.W., Maloney, E., Branson, M., 2020. Interactions between Moisture and Tropical Convection. Part I: The Coevolution of Moisture and Convection. *Journal of the Atmospheric Sciences* 77, 1783–1799. <https://doi.org/10.1175/JAS-D-19-0225.1>
- Xu, K., Hu, Y., Wong, T., 2019. Convective Aggregation and Indices Examined from CERES Cloud Object Data. *J. Geophys. Res. Atmos.* 124, 13604–13624. <https://doi.org/10.1029/2019JD030816>

ProQuest Number: 29215903

INFORMATION TO ALL USERS

The quality and completeness of this reproduction is dependent on the quality
and completeness of the copy made available to ProQuest.



Distributed by ProQuest LLC (2022).

Copyright of the Dissertation is held by the Author unless otherwise noted.

This work may be used in accordance with the terms of the Creative Commons license
or other rights statement, as indicated in the copyright statement or in the metadata
associated with this work. Unless otherwise specified in the copyright statement
or the metadata, all rights are reserved by the copyright holder.

This work is protected against unauthorized copying under Title 17,
United States Code and other applicable copyright laws.

Microform Edition where available © ProQuest LLC. No reproduction or digitization
of the Microform Edition is authorized without permission of ProQuest LLC.

ProQuest LLC
789 East Eisenhower Parkway
P.O. Box 1346
Ann Arbor, MI 48106 - 1346 USA